Journal of Nuclear Medicine, published on June 23, 2022 as doi:10.2967/jnumed.121.263330

^{89}Zr-labeled High-Density Lipoprotein Nanoparticle PET imaging reveals tumor uptake in patients with esophageal cancer

Running title: HDL PET imaging in esophageal cancer

Kang H. Zheng[1], Jeffrey Kroon[2], Jasper Schoormans[3], Oliver Gurney-Champion[4], Sybren L. Meijer[5], Suzanne S. Gisbertz[6], Maarten C.C.M. Hulshof[7], Danielle J. Vugts[8], Guus A.M.S. van Dongen[8], Bram F. Coolen[3], Hein J. Verberne[4], Aart J. Nederveen[4], Erik S.G. Stroes[1], Hanneke W.M. van Laarhoven[9]

Affiliations:

1. Department of Vascular Medicine, Amsterdam Cardiovascular Sciences, Amsterdam UMC, University of Amsterdam, Amsterdam, the Netherlands;
2. Department of Experimental Vascular Medicine, Amsterdam Cardiovascular Sciences, Amsterdam UMC, University of Amsterdam, the Netherlands;
3. Department of Biomedical Engineering & Physics, Amsterdam Cardiovascular Sciences, Amsterdam UMC, University of Amsterdam, Amsterdam, the Netherlands;
4. Department of Radiology and Nuclear Medicine, Amsterdam UMC, location Academic Medical Center, University of Amsterdam, Amsterdam, the Netherlands;
5. Department of Pathology, Cancer Center Amsterdam, Amsterdam UMC, University of Amsterdam, Amsterdam, the Netherlands;
6. Department of Surgery, Cancer Center Amsterdam, Amsterdam UMC, University of Amsterdam, Amsterdam, the Netherlands;
7. Department of Radiotherapy, Cancer Center Amsterdam, Amsterdam UMC, University of Amsterdam, Amsterdam, the Netherlands;
8. Department of Radiology and Nuclear Medicine, Amsterdam UMC, VU University, Amsterdam, the Netherlands;
9. Department of Medical Oncology, Cancer Center Amsterdam, Amsterdam UMC, University of Amsterdam, Amsterdam, the Netherlands

First author:

Kang H. Zheng, MD, PhD
Amsterdam UMC, Department of Vascular Medicine
Meibergdreef 9
1105 AZ Amsterdam
+31 20 566 6612
k.h.zheng@amsterdamumc.nl
ORCID: 0000-0001-8954-1337

Corresponding author:

Hanneke van Laarhoven, MD, PhD, PhD
Amsterdam UMC, Department of Medical Oncology
Meibergdreef 9
1105 AZ Amsterdam
+31 20 566 5957
h.vanlaarhoven@amsterdamumc.nl

Financial support: This work was supported by the Dutch Heart Foundation (CVON 2017-20: GENIUS-II). JK was supported by the Dutch Heart Foundation Senior Scientist Dekker grant (2021T045).

Key words: zirconium, PET/CT, high-density lipoprotein, nanomedicine, esophageal cancer

Abstract

Rationale: Nanomedicine holds promise for delivery of therapeutic and imaging agents to improve cancer treatment outcome. Preclinical studies demonstrated that high-density lipoprotein (HDL) nanoparticles accumulate in tumor tissue upon intravenous administration. Whether this HDL-based nanomedicine concept is feasible in patients is unexplored. Using a multi-modal imaging approach, we aimed to assess tumor uptake of exogenously administered HDL nanoparticles in patients with esophageal cancer.

Methods: The HDL mimetic CER-001 was radiolabeled using Zirconium-89 (^{89}Zr) to allow for PET/CT imaging. Patients with primary esophageal cancer staged T2 and above were recruited for serial ^{89}Zr-HDL PET/CT imaging prior to starting chemoradiation therapy. In addition, patients underwent routine ^{18}F-FDG PET/CT and 3T MRI scanning (DWI/IVIM and DCE-MRI) to assess tumor glucose metabolism, tumor cellularity and microcirculation perfusion, and tumor vascular permeability. Tumor biopsies were analyzed for expression of the HDL scavenger receptor class B1 (SR-B1) and macrophage marker CD68 using immunofluorescent staining.

Results: Nine patients with adenocarcinoma or squamous cell carcinoma underwent all study procedures. Following injection of ^{89}Zr-HDL (mean 39.2±1.2 MBq) , blood pool SUV_{mean} decreased over time (t=1h: 11.0±1.7; t=24h: 6.5±0.6; t=72h: 3.3±0.5), while liver and spleen SUV_{mean} remained relatively constant (t=1h: 4.1±0.6; t=24h: 4.0±0.8; t=72h: 4.3±0.8; and t=1h: 4.1±0.3; t=24h: 3.4±0.3; t=72h: 3.1±0.4, respectively) and kidney SUV_{mean} markedly increased over time (t=1h: 4.1±0.9; t=24h: 9.3±1.4; t=72h: 9.6±2.0). Tumor uptake increased over time (SUV_{peak} t=1h: 3.5±1.1; t=24h: 5.5±2.1 (p=0.016); t=72h: 5.7±1.4 (p=0.001)). The effective dose of ^{89}Zr-HDL was 0.523±0.040 mSv/MBq. No adverse events were observed after administration of ^{89}Zr-HDL. PET/CT and 3T MRI measures of tumor glucose metabolism, tumor cellularity and microcirculation perfusion, and tumor vascular permeability did not correlate with tumor uptake of ^{89}Zr-HDL, suggesting a specific mechanism to mediate the accumulation of ^{89}Zr-HDL. Immunofluorescent staining of clinical biopsies demonstrated SR-B1 and CD68 positivity in tumor tissue, establishing a potential cellular mechanism of action.

Conclusions: This was the first ^{89}Zr-HDL study in human oncology. ^{89}Zr-HDL PET/CT imaging demonstrates that intravenously administered HDL nanoparticles accumulate in tumors of

patients with esophageal cancer. The administration of ^{89}Zr-HDL was safe. These findings may support the development of HDL nanoparticles as a clinical delivery platform for drug agents. ^{89}Zr-HDL imaging may guide drug development and serve as biomarker for individualized therapy.

Graphical abstract

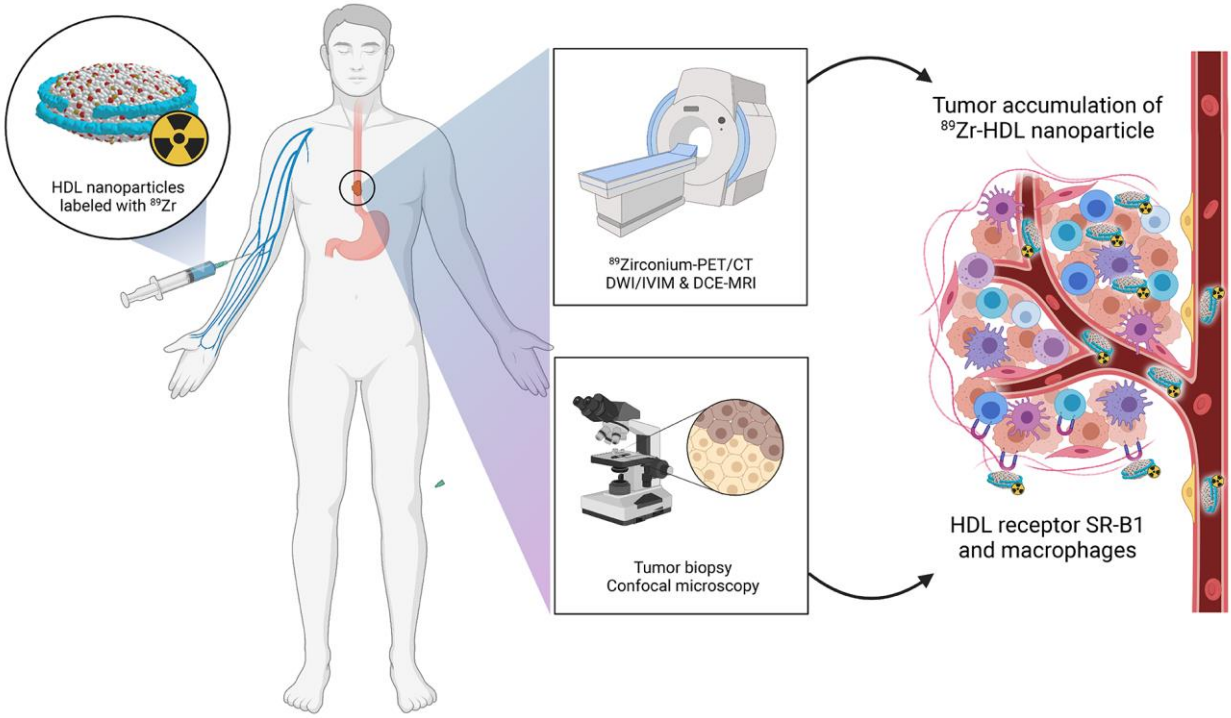

Introduction

Esophageal cancer is the sixth leading cause of death from cancer worldwide and represents a major healthcare problem (*1*). This malignancy is associated with substantial morbidity and has a dismal prognosis with a 5-year survival rate of less than 25% (*2*), despite advances in multimodality treatment strategies. Oncological treatment for esophageal carcinoma invariably involves the use of (preoperative) chemotherapy or concurrent chemoradiation (*3*). An important limitation of systemic chemotherapy is non-specificity, resulting in low intra-tumor drug concentrations while off-target cytotoxic effects limit the intensity of dosing. Novel treatment strategies are needed to improve efficacy and avoid toxicity in management of esophageal carcinoma.

Nanomedicine is an emerging approach to address the issues of poor outcome and limited efficacy in oncology (*4*). The key principle involves the use of nano-sized particles as vehicles for drug and/or imaging agents, to enhance delivery to tumors and avoid the first-pass clearance by the liver. Nanoparticles should improve the balance between local efficacy and systemic toxicity, as compared with conventional therapies such as systemic chemotherapy. Several innovative nanomedicines have been FDA-approved or reached clinical stage of development (*5*). Nevertheless, clinical breakthroughs in terms of significantly prolonging patient survival have not yet been achieved by the majority of nanoparticle platforms, comprising liposomes, albumin nanoparticles or micelles. This may be due to inherent limitations of these nanosystems to deal with the complexities and heterogeneity of tumor biology, relating to factors such as passive targeting, circulation half-life, tumor penetration, cellular uptake and drug release. Specific toxicity associated with certain nanoparticles, such as hypersensitivity reactions, may also hamper clinical development (*6*).

High-density lipoproteins (HDLs) have received considerable interest due to their potential for drug delivery and imaging (*7*). HDLs are endogenous, nano-sized carriers of cholesterol and one of their main physiological functions is considered to be the targeting and removal of cholesterol from peripheral tissues, including lipid-laden macrophages; followed by transportation to the liver for excretion (*8*). To exercise their function, HDLs have a natural conduit for interaction with peripheral cells through specific receptors, including scavenger receptor class B1 (SR-B1). HDLs can be formulated to carry therapeutic payloads, within their hydrophilic core or surface,

including hydrophobic drugs, controlled-released polymers and short interfering RNAs (*9*). These characteristics and the absence of specific toxicity may allow HDLs to overcome the barriers faced by other nanosystems. In support, administration of radiolabeled HDL nanoparticles in a mouse model of breast cancer resulted in accumulation in tumors, due to uptake in tumor associated macrophages (*10*).

We aimed to investigate this concept in patients and set out to assess whether administered HDL nanoparticles accumulate in primary esophageal tumors. To this end, we labeled the HDL mimetic CER-001 with Zirconium-89 (^{89}Zr-HDL) to allow for *in vivo* tracing using serial PET/CT imaging (*11*). Furthermore, we explored whether the tumor uptake of radiolabeled HDL was associated with [1] tumor metabolism, as assessed with routine ^{18}F-FDG PET/CT, [2] tumor diffusion and microcirculation perfusion, as assessed with diffusion weighted imaging/intravoxel incoherent motion imaging (DWI/IVIM), and [3] tumor vascular permeability, as assessed with dynamic contrast-enhanced magnetic resonance imaging (DCE-MRI). Finally, we investigated the presence of the HDL receptor SR-B1 and macrophages in tumor biopsies using immunofluorescence.

Materials and Methods

Study design

This study was a single-center prospective trial and was conducted in accordance to the principles of the Declaration of Helsinki. The protocol was approved by the local ethics committee and all participants provided written informed consent. Patients with esophageal cancer were included and visited the study center three times. All patients received a single injection of ^{89}Zr-HDL (CER-001 10 mg; 37 MBq), followed by serial PET/CT scanning at 1 hour, 24 hours and 72 hours post-administration. In addition, all patients were scanned on a 3T MRI scanner during one of the study visits.

Study population

Eligible patients were adult subjects with a primary esophageal carcinoma in situ prior to treatment, with a histopathological proven diagnosis and staged at least as locally advanced T2

(according to the TNM classification). Patients were recruited from the Gastro-Intestinal Oncology Center Amsterdam.

^{89}Zr-HDL and ^{18}F-FDG PET/CT

^{89}Zr-HDL was synthesized according to current Good Manufacturing Practice guidelines. The procedure for ^{89}Zr-radiolabeling of CER-001, as well as the quality and stability tests, have been described previously (*11*,*12*). The specific activity was 3.7 MBq ^{89}Zr per milligram CER-001. Radiochemical purity was determined using SE-HPLC (100±0%) and spin filters (99.3±0.4%). We demonstrated that covalent coupling of bifunctional chelator p-isothiocyanotobenzyl desferrioxamine (DFO-NCS) to CER-001 and subsequent labeling with Zirconium did not affect its functionality in vitro and in vivo. Whole body ^{89}Zr-HDL PET/CT scans were performed on a Siemens Biograph mCT Flow (Siemens, Munich, Germany). A low-dose CT scan was acquired with automatic modulation in current and voltage (reference values: 120 kV and 50 mA, 128x0.6 collimation and 0.9 pitch). PET imaging was performed with continuous bed motion 1.1 mm/s (legs) and 0.7 mm/s (body) in 3D acquisition mode. CT data was used for PET attenuation correction and PET data were reconstructed with TrueX algorithm (three dimensions ordered subsets expectation maximization iterative reconstruction with time of flight and point spread function compensation, 21 subsets, 2 iterations, and a 5 mm Gaussian post-filter) in 4 × 4 × 5 mm voxels.

^{18}F-FDG PET/CT scans were acquired according to the local clinical protocol, using the same Siemens Biograph mCT Flow. Patients were instructed to drink 2 liters of water and to not perform strenuous physical activities in the 24 hours preceding the scan. Patients were fasted for at least 6 hours except for glucose-free oral hydration before intravenous administration of ^{18}F-FDG. Prior to ^{18}F-FDG administration, fasting capillary blood glucose concentrations were measured with a blood glucose meter (StatStrip, Nova Biomedical Corporation, Waltham, MA, USA). Dosages of ^{18}F-FDG ranged from 180 to 400 MBq depending on body mass index. PET/CT scanning was performed 60 min after injection of ^{18}F-FDG. A diagnostic CT scan was acquired with automatic modulation in current and voltage (reference values: 120 kV and 160 mA, 128x0.6 collimation and 0.9 pitch) after intravenous administration of iodinated contrast medium (100 mL Ultravist 300; Bayer Healthcare Pharmaceuticals, Berlin) with a flow of 3 mL/sec and a 65 second delay (portal phase). PET imaging was performed with continuous bed

motion at 1.5 mm/sec in 3D acquisition mode. CT data was used for PET attenuation correction and PET data were reconstructed with TrueX algorithm (three dimensions ordered subsets expectation maximization iterative reconstruction with time of flight and point spread function compensation, 21 subsets, 2 iterations, and a 5 mm Gaussian post-filter) in 4 mm × 4 mm × 5 mm voxels.

Image analysis was performed on a dedicated commercially available workstation (OsiriX, Pixmeo, Switzerland and OLINDA/EXM, Hermes Medical Solutions, Stockholm, Sweden). Tumor and organ uptake were assessed by manually drawing regions of interest delineating the whole tumor or organ (in all slices where visible) on the co-registered CT. Blood pool activity was determined by drawing regions of interest in 5 contiguous axial slices in the lumen of the superior vena cava. The maximal standardized uptake value (SUV_{max}) was calculated as the maximal pixel activity within each region of interest. For tumors, the peak standardized uptake value (SUV_{peak}) was calculated at the mean pixel activity within a volume of interest (1 cm^3) centered around the hottest pixel value. The target-to-blood pool ratio (TBR) was calculated by dividing the standardized uptake value by the mean blood pool activity. The internal radiation dosimetry for the adult human was evaluated through the normalized cumulated activities for each patient, provided as input to the OLINDA/EXM code. Residence times were calculated for the liver, kidney, lungs, spleen and the remainder of the body, entering the percentage of the injected dose at each time point for each patient in OLINDA/EXM and fitting these data using a mono-exponential function.

3T MRI acquisition and analysis

Patients were scanned on a 3T MRI scanner (Philips Ingenia, Best, The Netherlands) with an anterior 16-channel phased-array coil and a posterior 16-channel phased-array coil. The scanner's maximum gradient strength was 45 mT/m and maximum slew rate was 200 T/m/s. Three-dimensional T1w 3-point Dixon and multi-slice T2w TSE images were obtained for reference.

DWI/IVIM - Axial diffusion-weighted 2D multi-slice single shot echo-planar imaging with SPIR fat suppression was performed with the following acquisitions settings: TR/TE = 4600/70 ms, FOV = 350x160 mm, resolution = 2.2x2.2 mm^2 (1.8x1.8 mm^2 reconstructed), number of slices = 20, slice thickness = 4.5 mm (slice gap = 0.5 mm), SENSE factor = 1.4, EPI bandwidth = 16.5

Hz/voxel, b-values = 0 (3 averages), 100 (6 averages), 800 (10 averages) s/mm^2. Scans were respiratory triggered by means of using a liver-lung interface navigator signal.

From the DW images, parameter maps were calculated for diffusivity (*D*) and perfusion fraction (*f*) in Matlab 2016a (Mathworks, Natick, MA, USA) based on in house software (*13,14*), adapted to work for 3-b values. The diffusivity was calculated voxel-wise taking a least-squares fit to the DWI data from b-values 100 and 800 s/mm^2:

$$S(b) = S0' \times e^{-b \times D}, \quad [1]$$

where S(b) is the signal at b-value b. S0' is the extrapolated signal at b=0 s/mm^2, if the data were mono-exponential. The difference between the measured S (b=0 s/mm^2) and S0', in turn, relates to the perfusion fraction as:

$$f = 1 - \frac{S0'}{S(b=0)}. \quad [2]$$

Regions of interest were drawn on the b=800 s/mm^2 and propagated to the parameters maps to assess parameter values inside the tumor regions.

DCE-MRI - For dynamic contrast-enhanced MRI, a highly accelerated golden angle radial stack-of-stars TFE sequence (*15*) was performed continuously at a temporal resolution of 8.7 seconds per time frame. Two minutes after the start of the scan, a Gd-based contrast agent (Gadovist, Bayer, Leverkusen, Germany) at the dose of 0.1 mmol/kg bodyweight was injected intravenously at 2 ml/sec. Other relevant scan parameters were: TR/TE =7.5/3.4 ms, flip angle = 11 degrees; spatial resolution: 1x1x2 mm^3.

The undersampled data was reconstructed in Matlab 2016a using compressed sensing (ref) with total variation regularization in the time domain (lambda=0.01) and 100 iterations. Frame-by-frame tumor segmentation was performed on the dynamic data with ImageJ (U. S. National Institutes of Health, Bethesda, Maryland, USA). Signal-intensity curves were obtained from the time series, and the area-under-the-curve (AUC) was calculated for the first two minutes after contrast injection as a semi-quantitative measure of tumor permeability.

Histology and immunohistochemistry

Tumor biopsies were obtained during routine clinical workup before start of neoadjuvant treatment and cut into slices. All samples were stained with hematoxylin and eosin for general morphology. For immunohistochemistry, the slides were dewaxed to remove the paraffin, followed by antigen retrieval using the LabVision PT module (ThermoFisher Scientific) at pH 6.0 for 20 min at 98 °C. Next, the slides were washed with PBS for three times and blocked with Ultravision protein block (TA-125-PBQ; ThermoFisher Scientific) for 10 minutes at room temperature. Slides were incubated with primary antibodies: SR-B1 (NB400-101; Novus Biologicals), CD68 (clone KP-1, cat number Ab955; Abcam). Consequently, secondary antibodies Alexa Fluor-488 (A21121; Invitrogen) and Alexa Fluor-568 (A11036; Invitrogen) were used. Cells were embedded using Prolongold (P36935; ThermoFisher Scientific), containing DAPI. Imaging was performed on the Leica DMI6000 (SP8) confocal microscope using a 63x objective. Positive pixels for either SR-B1 or CD68 per tumor biopsy, were normalized for nuclear content (using DAPI), in order to normalize cellular biopsy area using Fiji (ImageJ v2.1.0/1.53c). Percentage of colocalization between SR-B1 and CD68 refers to the percentage of pixels of the total number of pixels per image and is determined using Fiji's Coloc 2 plugin.

Statistical analysis

All data are presented as mean with standard deviation. For evaluation of ^{89}Zr-HDL uptake over time, a repeated measures one-way analysis of variance was performed (significance level alpha=0.05). If significance was found, post-hoc testing with Bonferroni correction was performed to assess the difference in uptake compared with the first timepoint. Correlation between ^{89}Zr-HDL uptake, MRI parameters and immunohistochemistry data was tested using Pearson's correlation coefficients. Statistical analyses were performed using the SPSS Statistics package version 26 (IBM, Armonk, New York).

Results

We recruited 9 male patients with a mean age of 66±9 years, of whom 7 (78%) were recently diagnosed with adenocarcinoma and 2 (22%) with squamous-cell carcinoma of the esophagus. Baseline characteristics are listed in Table 1. All patients received an injection of 10 mg of ^{89}Zr-HDL (mean 39.2±1.2 MBq) and underwent serial PET/CT and 3T MRI scanning before starting chemo-radiation therapy. PET/CT scanning was performed at t=1h (1h:03m±0h:07m), t=24h (24h:41m±0h:28m) and t=72h (71h:11m±2h:06m) after injection of ^{89}Zr-HDL. ^{89}Zr-HDL was well-tolerated during the study and no adverse events were reported.

Biodistribution and radiation dosimetry of ^{89}Zr-HDL

Following injection of ^{89}Zr-HDL, serial PET/CT imaging was performed at 1 hour, 24 hours and 72 hours post-injection. Visual inspection revealed clear radiotracer signal in the blood pool, liver, spleen and kidneys (Figure 1). Uptake of ^{89}Zr-HDL was measured in selected source organs (Supplemental Figure 1). Blood pool SUV_{mean} was 11.0±1.7 at 1 hour after administration, which decreased to 6.5±0.6 at 24 hours and 3.3±0.5 at 72 hours (both $p < 0.0001$). Liver SUV_{mean} was 4.1±0.6 at 1 hour and remained constant over time, whereas spleen signal decreased slightly from 4.1±0.3 to 3.4±0.3 and 3.1±0.4, after 24 and 72 hours respectively ($p <0.001$). Kidney SUV_{mean} markedly increased from 4.1±0.9 to 9.3±1.4 after 24 hours and remained elevated at 72 hours ($p<0.0001$), confirming the kidneys to be the major site of catabolism of HDL. Organ dosimetry data and residence times are listed in Supplemental Table 1. The organs with the highest absorbed dose were the stomach (0.086±0.013 mSv/MBq), lungs (0.070±0.008 mSv/MBq) and liver (0.053±0.010 mSv/MBq).

PET/CT imaging of esophageal tumors

We used clinical ^{18}F-FDG PET/CT scans to assist in delineating the esophageal tumors, which demonstrated intense ^{18}F-FDG uptake as expected (Figure 2A+B). On co-localized ^{89}Zr-HDL PET/CT scans, focal uptake patterns in the esophageal tumors could clearly be observed from 24 hours onwards (Figure 2A). Considering the relatively small size of esophageal tumors (mean 48.0±26.6 cm^3) and the focal uptake patterns, the tumor uptake of ^{89}Zr-HDL was reported using SUV_{peak} as a more robust quantification as compared with the SUV_{max}. The tumor uptake of ^{89}Zr-

HDL increased significantly at 24 and 72 hours for all tumors, compared with 1 hour after injection (SUV_{max} t=1h: 6.1±1.4; t=24h: 9.2±4.2 (p=0.036); t=72h: 10.2±3.4 (p=0.023); SUV_{peak} t=1h: 3.5±1.1; t=24h: 5.5±2.1 (p=0.016); t=72h: 5.7±1.4 (p=0.001) (Figure 2C)). When corrected for the blood pool, the tumor target-to-blood pool ratio increased significantly over time (TBR_{peak} t=1h: 0.3±0.1; t=24h: 0.9±0.3 p<0.001; t=72h: 1.8±0.5 (p<0.001)). There was no association between tumor uptake values ^{18}F-FDG and ^{89}Zr-HDL (Figure 2D).

DWI/IVIM and DCE-MRI of esophageal tumors

To explore whether characteristics of the tumor microenvironment affect the ability of HDL nanoparticles to penetrate tumors, all patients underwent DWI/IVIM and DCE-MRI scanning. We localized the tumors using T2w TSE images (Figure 3A). DWI/IVIM images were acquired and parameter maps of diffusivity and perfusion fraction were generated (Figure 3B). Mean values of diffusivity and perfusion fraction of the tumors were not associated with tumor uptake of ^{89}Zr-HDL (Figure 3C). DCE-MRI time series were obtained and quantitative pixel-wise AUC maps calculated from the first two minutes following Gadovist injection (Figure 3D). Mean AUC values of the tumors, as measure of permeability, were not associated with tumor uptake of ^{89}Zr-HDL uptake (Figure 3E).

HDL receptor expression in tumor biopsies

Histologic analysis of tumor biopsies from all patients was performed to assess general morphology (Figure 4A), the expression of the HDL receptor SR-B1 and presence of macrophage marker CD68 (Figure 4B). We established and quantified the presence of SR-B1 positive cells and macrophages by CD68 expression (Figure 4C), as well as cells with double positivity for these markers (Figure 4D). There was no relationship between semi-quantitative measures of SR-B1 and CD68 expression and tumor uptake of ^{89}Zr-HDL (Supplemental Figure 2).

Discussion

We report for the first time the uptake of HDL nanoparticles in tumors of patients with primary esophageal cancer. Following administration of ^{89}Zr-HDL, serial PET/CT demonstrated accumulation of HDL nanoparticles in the esophageal tumors over time. Tumor uptake could be quantified in all patients and no adverse events occurred. These findings herald clinical utility for HDL-based nanomedicine to target esophageal tumors for delivery of anticancer drugs.

In this proof-of-concept study, we applied ^{89}Zr-labeling to the HDL mimetic CER-001, which consists of recombinant apolipoprotein A-I and phospholipids. Our data indicated relatively low uptake in liver and spleen, while radiotracer signal increased in the kidneys over time. This finding is in line with the known renal catabolism of apolipoprotein A-I (*16*). Importantly, focal accumulation patterns of ^{89}Zr-HDL were observed in all esophageal tumors after 24 and 72 hours. These data highlight the translational potential of HDL nanoparticles as a tool for altering the biodistribution of drugs of interest, in order to achieve higher intra-tumor concentrations and to avoid systemic toxicity. This concept is supported by previous experimental studies in cardiovascular disease, which established that HDL nanoparticles effectively delivered their drug payload to atherosclerotic plaques (*17*,*18*).

The extravasation of nanoparticles to tumors is traditionally considered to depend on passive accumulation via the enhanced permeability and retention (EPR) effect (*19*). This phenomenon dictates that drug penetration in tumors is dependent on features of the tumor microenvironment, including the degree of cellularity and composition of extracellular matrix, as well as vascular permeability. Nevertheless, we found that tumor uptake of ^{89}Zr-HDL was not associated with imaging measures of tumor diffusivity (DWI/IVIM), nor with tumor perfusion (DWI/IVIM), or vascular permeability (DCE-MRI). These findings suggest the contribution of a specific mechanism mediating the accumulation HDL nanoparticles in esophageal cancer, rather than dependence on only passive vascular leakage.

We substantiated the presence of the HDL receptor SR-B1 in tumor biopsies of the studied patients, which could facilitate a specific mechanism for accumulation of HDL. Enhanced expression of SR-B1 has been suggested to be a mechanism for tumor cells to satisfy their increased demand for cholesterol to allow for proliferation and increased metabolic cellular processes (*20*). The level of SR-B1 expression in human breast and prostate cancer is associated

with tumor aggressiveness and adverse prognosis (*21*,*22*), while a variety of malignant cell lines overexpress SR-B1 (*20*). Yet, we did not find an association between tumor uptake of ^{89}Zr-HDL and tumor glycolytic activity (related to cellular proliferation) as measured with ^{18}F-FDG PET/CT. Prior studies using murine breast cancer models suggest that injected HDL nanoparticles are preferentially taken up by tumor associated macrophages (*10*,*23*), which may also express SR-B1 or other scavenger receptors for HDL. However, we found that colocalization of SR-B1 with CD68 was limited, suggesting cells other than macrophages could be responsible for the majority of uptake of HDL particles. Additional studies are needed to assess the cellular distribution of administered HDL particles in patients with esophageal cancer, as well as the cellular mechanisms involved. Collectively, ^{89}Zr-HDL PET/CT has potential to serve as a specific imaging biomarker to predict efficacy of HDL-mediated drug delivery (*24*).

For the first time, we reported radiation dosimetry of ^{89}Zr-HDL. The effective dose of ^{89}Zr-HDL (0.523 mSv/MBq) clearly exceeds that of the conventional diagnostic tracer ^{18}F-FDG (0.019 mSv/MBq) (*25*), although it is comparable to other ^{89}Zr-immunoPET tracers (*26*). While this may limit repetitive use, considering the poor survival rate of esophageal cancer, the risks of radiation may be acceptable when weighed against any potential future improvements in clinical treatment provided by this imaging modality.

We acknowledge several limitations of this study. As a pilot study, the sample size was small and carries the risk of a false negative finding in our correlation testing between imaging modalities. Spatial heterogeneity of tumors may have obscured MRI parameters which were calculated by averaging measurements in a region of interest. Finally, biopsies of tumors may not adequately reflect the tissue distribution of the tumor.

Conclusions

^{89}Zr-labeling of an HDL nanoparticle allowed for in vivo tracing using PET/CT in patients with esophageal cancer. Administration of ^{89}Zr-HDL was safe and the effective dose was in the range of other ^{89}Zr-tracers. Focal uptake patterns were observed within the esophageal tumors. Further studies are now needed to gain insight in the mechanisms of HDL accumulation in tumors and test the feasibility of HDL nanoparticles to serve as a delivery system for anticancer drugs.

Acknowledgements

The authors thank E. Poel, M.F. Lam and S.R. Havik for their invaluable technical assistance.

Disclosures

This is an investigator-initiated study, for which Cerenis provided CER-001. E.S. also served as principal investigator for the MODE, SAMBA and TANGO studies (involving CER-001). No other potential conflicts of interest relevant to this article exist.

Key points

Question:

Do intravenously administered HDL nanoparticles accumulate in tumors in patients with primary esophageal cancer?

Pertinent findings:

This prospective imaging study used ^{89}Zr-labeling of HDL nanoparticles to demonstrate accumulation in tumors of patients with esophageal cancer following intravenous administration (SUV_{peak} t=1h: 3.5±1.1; t=24h: 5.5±2.1; t=72h: 5.7±1.4). Tumor uptake of ^{89}Zr-HDL was not associated with measures from ^{18}F-FDG PET/CT, DWI/IVIM and DCE-MRI, suggesting a specific mechanism to mediate the accumulation of ^{89}Zr-HDL. Analysis of tumor biopsies showed the presence of SR-B1 positive cells and macrophages, indicating a potential mechanism of action.

Implications for patient care:

HDL nanoparticles hold potential to serve as a delivery system for anticancer drugs in esophageal cancer.

References

1. Smyth EC, Lagergren J, Fitzgerald RC, et al. Oesophageal cancer. *Nat Rev Dis Primers.* 2017;3:17048.

2. van Putten M, de Vos-Geelen J, Nieuwenhuijzen GAP, et al. Long-term survival improvement in oesophageal cancer in the Netherlands. *Eur J Cancer.* 2018;94:138-147.

3. Shah MA, Kennedy EB, Catenacci DV, et al. Treatment of Locally Advanced Esophageal Carcinoma: ASCO Guideline. *J Clin Oncol.* 2020;38:2677-2694.

4. Shi J, Kantoff PW, Wooster R, Farokhzad OC. Cancer nanomedicine: progress, challenges and opportunities. *Nat Rev Cancer.* 2017;17:20-37.

5. Tran S, DeGiovanni PJ, Piel B, Rai P. Cancer nanomedicine: a review of recent success in drug delivery. *Clin Transl Med.* 2017;6:44.

6. Szebeni J, Simberg D, Gonzalez-Fernandez A, Barenholz Y, Dobrovolskaia MA. Roadmap and strategy for overcoming infusion reactions to nanomedicines. *Nat Nanotechnol.* 2018;13:1100-1108.

7. Lobatto ME, Fuster V, Fayad ZA, Mulder WJ. Perspectives and opportunities for nanomedicine in the management of atherosclerosis. *Nat Rev Drug Discov.* 2011;10:835-852.

8. Ouimet M, Barrett TJ, Fisher EA. HDL and Reverse Cholesterol Transport. *Circ Res.* 2019;124:1505-1518.

9. Mulder WJM, van Leent MMT, Lameijer M, Fisher EA, Fayad ZA, Perez-Medina C. High-Density Lipoprotein Nanobiologics for Precision Medicine. *Acc Chem Res.* 2018;51:127-137.

10. Perez-Medina C, Tang J, Abdel-Atti D, et al. PET Imaging of Tumor-Associated Macrophages with 89Zr-Labeled High-Density Lipoprotein Nanoparticles. *J Nucl Med.* 2015;56:1272-1277.

11. Zheng KH, van der Valk FM, Smits LP, et al. HDL mimetic CER-001 targets atherosclerotic plaques in patients. *Atherosclerosis.* 2016;251:381-388.

12. Vosjan MJ, Perk LR, Visser GW, et al. Conjugation and radiolabeling of monoclonal antibodies with zirconium-89 for PET imaging using the bifunctional chelate p-isothiocyanatobenzyl-desferrioxamine. *Nat Protoc.* 2010;5:739-743.

13. Gurney-Champion OJ, Froeling M, Klaassen R, et al. Minimizing the Acquisition Time for Intravoxel Incoherent Motion Magnetic Resonance Imaging Acquisitions in the Liver and Pancreas. *Invest Radiol.* 2016;51:211-220.

14. Klaassen R, Gurney-Champion OJ, Engelbrecht MRW, et al. Evaluation of Six Diffusion-weighted MRI Models for Assessing Effects of Neoadjuvant Chemoradiation in Pancreatic Cancer Patients. *Int J Radiat Oncol Biol Phys.* 2018;102:1052-1062.

15. Zheng KH, Schoormans J, Stiekema LCA, et al. Plaque Permeability Assessed With DCE-MRI Associates With USPIO Uptake in Patients With Peripheral Artery Disease. *JACC Cardiovasc Imaging.* 2019;12:2081-2083.

16. Moestrup SK, Nielsen LB. The role of the kidney in lipid metabolism. *Curr Opin Lipidol.* 2005;16:301-306.

17. Duivenvoorden R, Tang J, Cormode DP, et al. A statin-loaded reconstituted high-density lipoprotein nanoparticle inhibits atherosclerotic plaque inflammation. *Nat Commun.* 2014;5:3065.

18. Kim Y, Lobatto ME, Kawahara T, et al. Probing nanoparticle translocation across the permeable endothelium in experimental atherosclerosis. *Proc Natl Acad Sci U S A.* 2014;111:1078-1083.

19. Prabhakar U, Maeda H, Jain RK, et al. Challenges and key considerations of the enhanced permeability and retention effect for nanomedicine drug delivery in oncology. *Cancer Res.* 2013;73:2412-2417.

20. Mooberry LK, Sabnis NA, Panchoo M, Nagarajan B, Lacko AG. Targeting the SR-B1 Receptor as a Gateway for Cancer Therapy and Imaging. *Front Pharmacol.* 2016;7:466.

21. Schorghofer D, Kinslechner K, Preitschopf A, et al. The HDL receptor SR-BI is associated with human prostate cancer progression and plays a possible role in establishing androgen independence. *Reprod Biol Endocrinol.* 2015;13:88.

22. Yuan B, Wu C, Wang X, et al. High scavenger receptor class B type I expression is related to tumor aggressiveness and poor prognosis in breast cancer. *Tumour Biol.* 2016;37:3581-3588.

23. Mason CA, Kossatz S, Carter LM, et al. An (89)Zr-HDL PET Tracer Monitors Response to a CSF1R Inhibitor. *J Nucl Med.* 2020;61:433-436.

24. Jauw YW, Menke-van der Houven van Oordt CW, Hoekstra OS, et al. Immuno-Positron Emission Tomography with Zirconium-89-Labeled Monoclonal Antibodies in Oncology: What Can We Learn from Initial Clinical Trials? *Front Pharmacol.* 2016;7:131.

25. Mattsson S, Johansson L, Leide Svegborn S, et al. Radiation Dose to Patients from Radiopharmaceuticals: a Compendium of Current Information Related to Frequently Used Substances. *Ann ICRP.* 2015;44:7-321.

26. Borjesson PK, Jauw YW, de Bree R, et al. Radiation dosimetry of 89Zr-labeled chimeric monoclonal antibody U36 as used for immuno-PET in head and neck cancer patients. *J Nucl Med.* 2009;50:1828-1836.

Figure 1. ^{89}Zr-HDL PET images

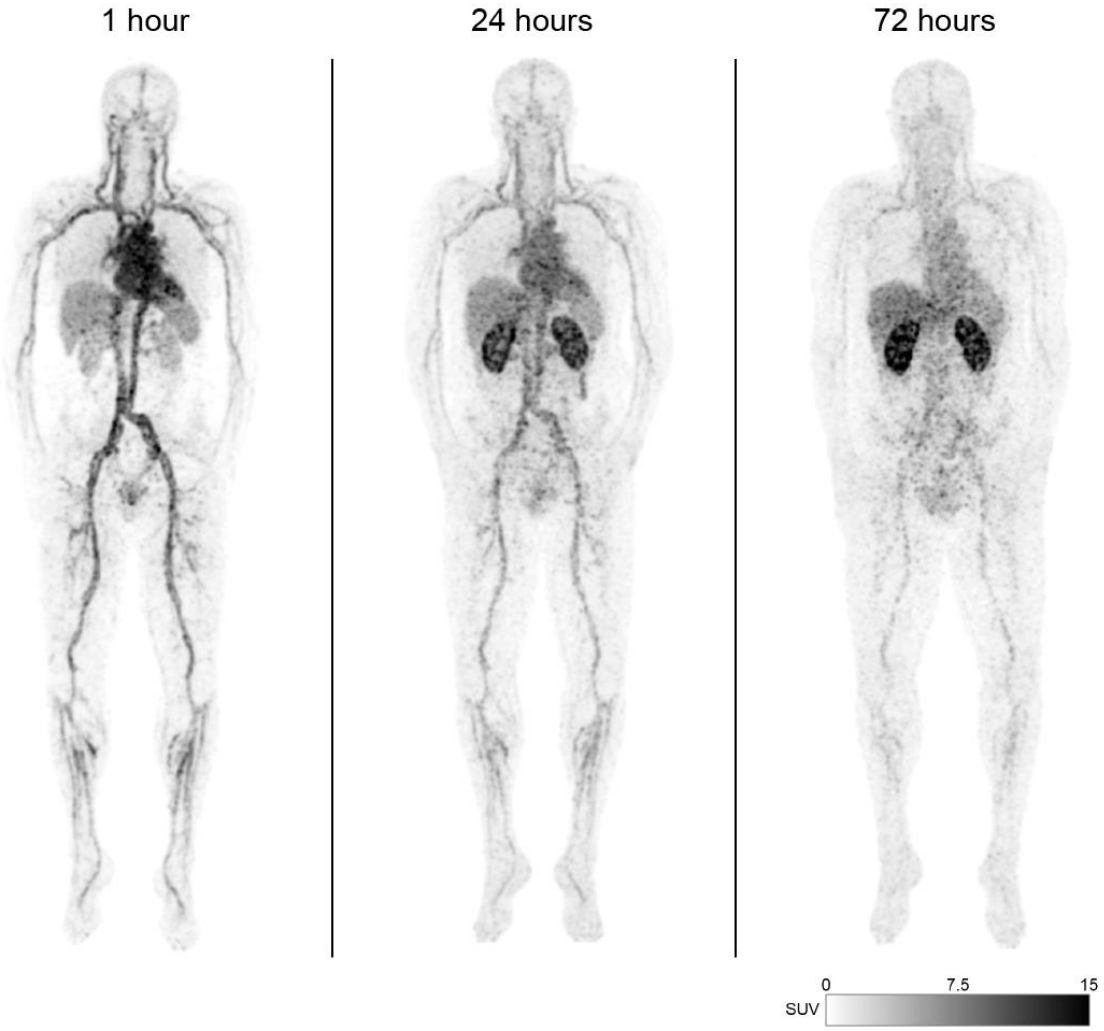

Maximum intensity projections of serial ^{89}Zr-HDL PET scans (Subject #ID 01).

Figure 2. PET/CT imaging of esophageal carcinoma

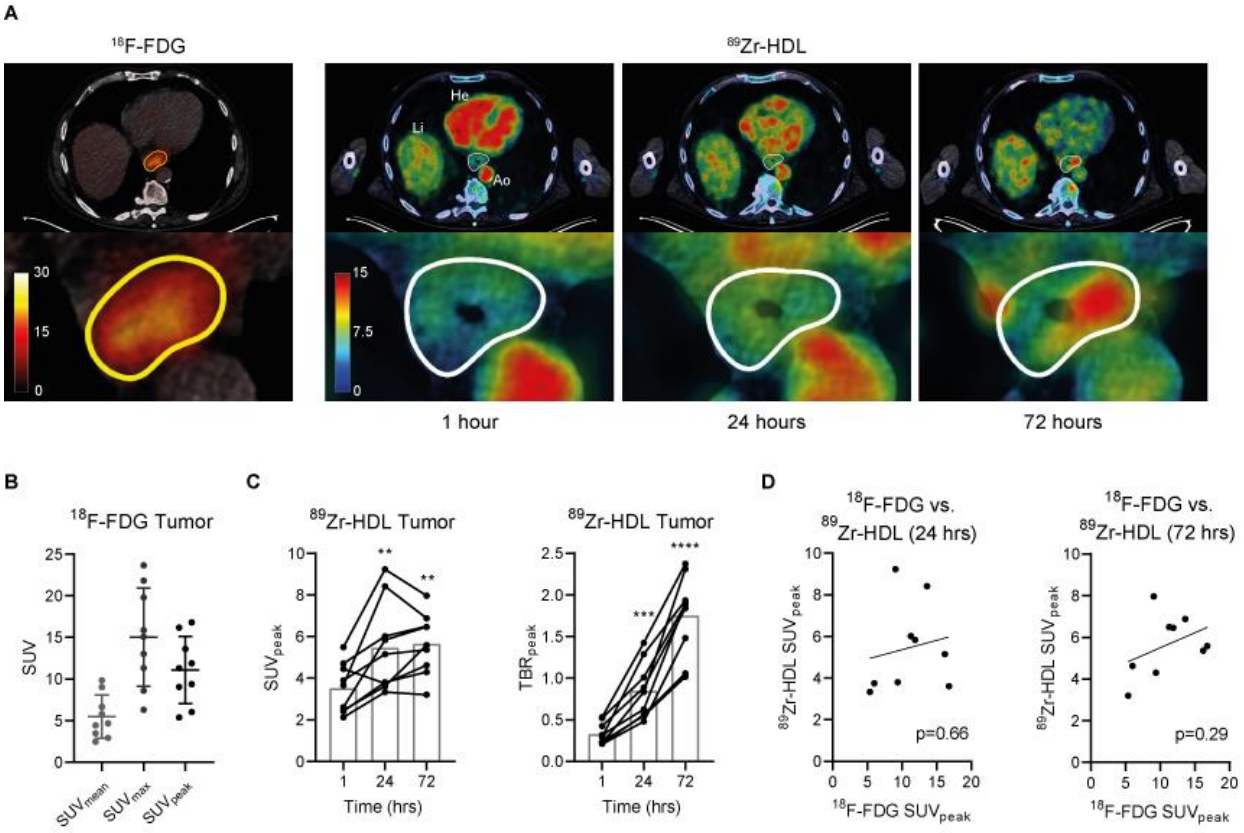

PET/CT images from a subject (ID# 06) with esophageal adenocarcinoma. **(A, B)** ^{18}F-FDG uptake was clearly increased in the tumors. Upon administration of ^{89}Zr-HDL, signal intensity in the esophageal tumor increases over time and a focal uptake pattern can be clearly visualized in this subject at 72 hours. **(C)** Tumor standardized uptake values and target-to-blood pool ratios increase over time, indicating the accumulation of ^{89}Zr-HDL particles in the tumors. **(D)** There was no association between ^{18}F-FDG and ^{89}Zr-HDL uptake in tumors.
Ao = aorta, He = heart, Li = liver.

Figure 3. DWI/IVIM and DCE-MRI

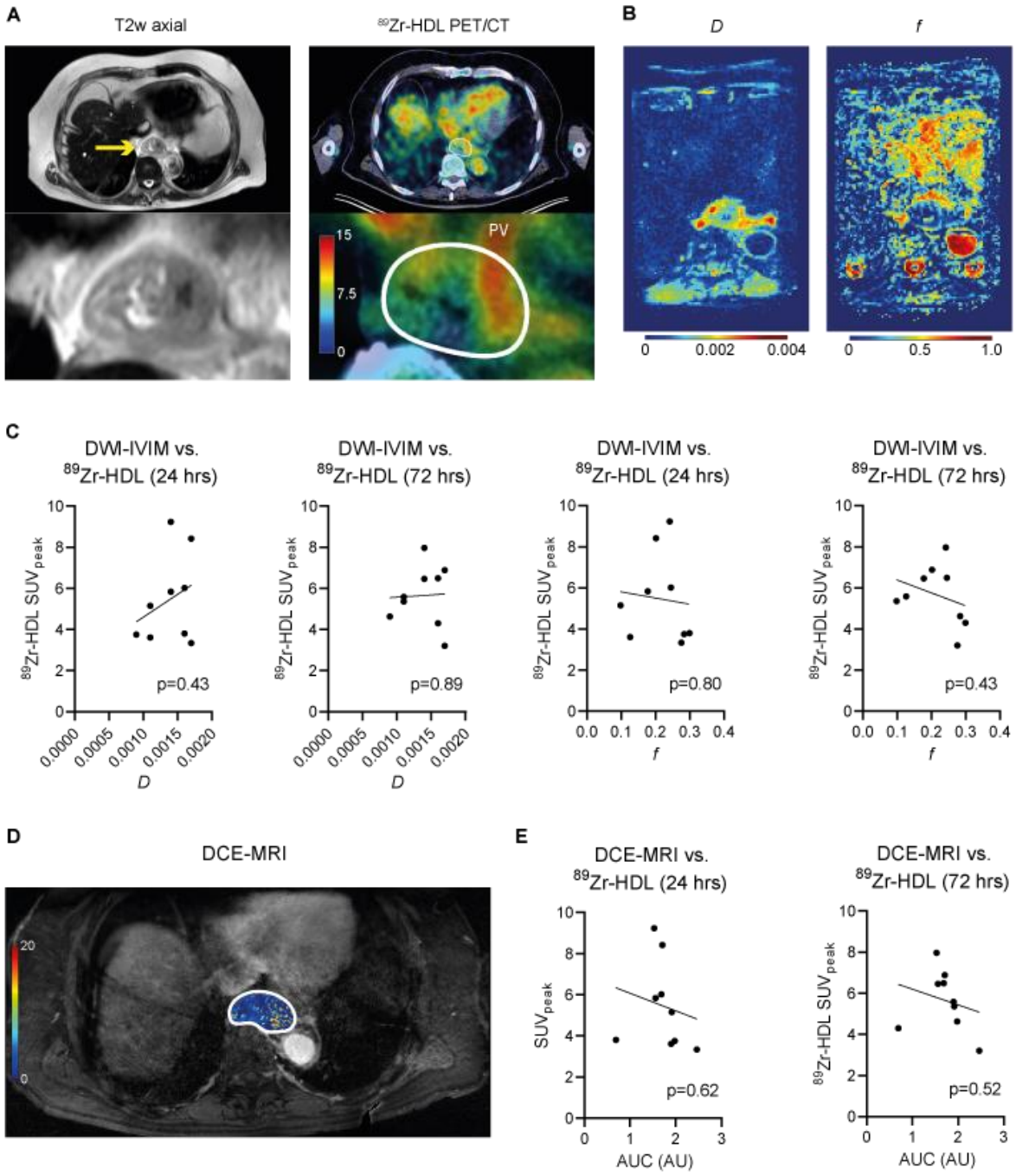

Patients underwent DWI/IVIM and DCE-MRI scanning (Subject #ID 07). **(A)** Left panel: T2w TSE images were obtained to localize the tumors. Yellow arrow indicates tumor. Right panel: corresponding ^{89}Zr-HDL PET/CT at 72 hours, with focal uptake in the tumor delineated with white line, as well as intravascular signal from the adjacent pulmonary vein (PV). **(B)** DWI/IVIM images were acquired in order to generate diffusivity and perfusion fraction maps. **(C)** Mean *D* and *f* values calculated from the parameter maps were not associated with tumor uptake of ^{89}Zr-HDL. **(D)** Quantitative AUC maps resulting from DCE-MRI time series. **(E)** Mean AUC values were not associated with tumor uptake of ^{89}Zr-HDL.

Figure 4. HDL receptor expression and macrophage presence in tumor biopsies

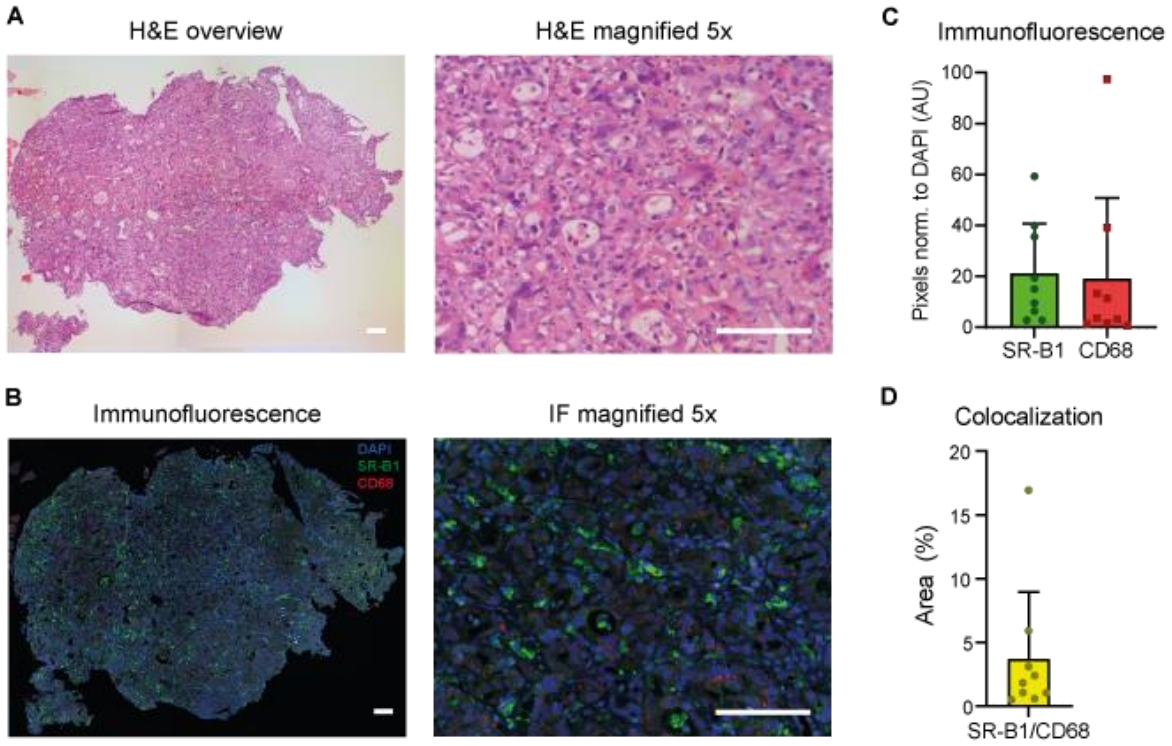

Histology and immunofluorescence of tumor biopsies before chemoradiation therapy (Subject #ID 03). **(A)** Hematoxylin and eosin staining with **(B)** corresponding confocal microscopy image for DAPI (blue), SR-B1 (green) and CD68 (red). **(C)** Pixel count of SR-B1 and CD68 normalized to DAPI. **(D)** Percent area with double positivity for SR-B1 and CD68.

Table 1. Baseline characteristics

#ID	Age (yrs)	Sex (M/F)	BMI (kg/m^2)	Tumor type	Tumor size (cm^3)	Tumor stage
01	73	M	26,7	Adenocarcinoma	20,4	T2N1M0
02	62	M	31,4	Adenocarcinoma	71,2	T3N1M0
03	68	M	19,4	Adenocarcinoma	16,2	T3N0M0
04	67	M	24,7	Squamous-cell	97,3	T2N1M0
05	57	M	24,4	Adenocarcinoma	49,0	T3N2M1
06	66	M	26,1	Adenocarcinoma	53,7	T3N2M0
07	82	M	28,1	Adenocarcinoma	52,8	T3N1M0
08	51	M	28,1	Squamous-cell	19,2	T3N2M0
09	66	M	30,4	Adenocarcinoma	52,8	T3N0M0

Baseline characteristics of included patients. Tumors were classified according to TNM Staging System.

SUPPLEMENTAL DATA

^{89}Zr-labeled High-Density Lipoprotein Nanoparticle PET imaging reveals tumor uptake in patients with esophageal cancer

Kang H. Zheng[1], Jeffrey Kroon[2], Jasper Schoormans[3], Oliver Gurney-Champion[4], Sybren L. Meijer[5], Suzanne S. Gisbertz[6], Maarten C.C.M. Hulshof[7], Danielle J. Vugts[8], Guus A.M.S. van Dongen[8], Bram F. Coolen[3], Hein J. Verberne[4], Aart J. Nederveen[4], Erik S.G. Stroes[1], Hanneke W.M. van Laarhoven[9]

Affiliations:

1. Department of Vascular Medicine, Amsterdam Cardiovascular Sciences, Amsterdam UMC, University of Amsterdam, Amsterdam, the Netherlands;
2. Department of Experimental Vascular Medicine, Amsterdam Cardiovascular Sciences, Amsterdam UMC, University of Amsterdam, the Netherlands;
3. Department of Biomedical Engineering & Physics, Amsterdam Cardiovascular Sciences, Amsterdam UMC, University of Amsterdam, Amsterdam, the Netherlands;
4. Department of Radiology and Nuclear Medicine, Amsterdam UMC, location Academic Medical Center, University of Amsterdam, Amsterdam, the Netherlands;
5. Department of Pathology, Cancer Center Amsterdam, Amsterdam UMC, University of Amsterdam, Amsterdam, the Netherlands;
6. Department of Surgery, Cancer Center Amsterdam, Amsterdam UMC, University of Amsterdam, Amsterdam, the Netherlands;
7. Department of Radiotherapy, Cancer Center Amsterdam, Amsterdam UMC, University of Amsterdam, Amsterdam, the Netherlands;
8. Department of Radiology and Nuclear Medicine, Amsterdam UMC, VU University, Amsterdam, the Netherlands;
9. Department of Medical Oncology, Cancer Center Amsterdam, Amsterdam UMC, University of Amsterdam, Amsterdam, the Netherlands

Supplemental Figure 1. Biodistribution of ^{89}Zr-HDL

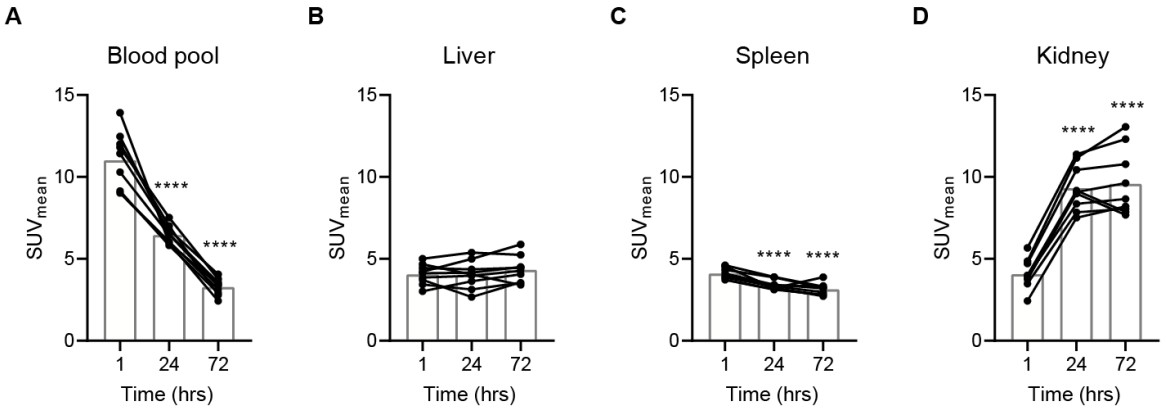

Standardized uptake values were calculated in source organs. Each line represents an individual subject. **(A)** Blood pool activity decreased between 1 and 72 hours, compared with 1 hour after injection. **(B)** Liver uptake remained stable. **(C)** Spleen uptake slightly decreased over time. **(D)** Kidney uptake increased between 1 and 24 hours after injection and remained elevated at 72 hours.

Supplemental Figure 2. HDL receptor expression and macrophage presence in tumor biopsies

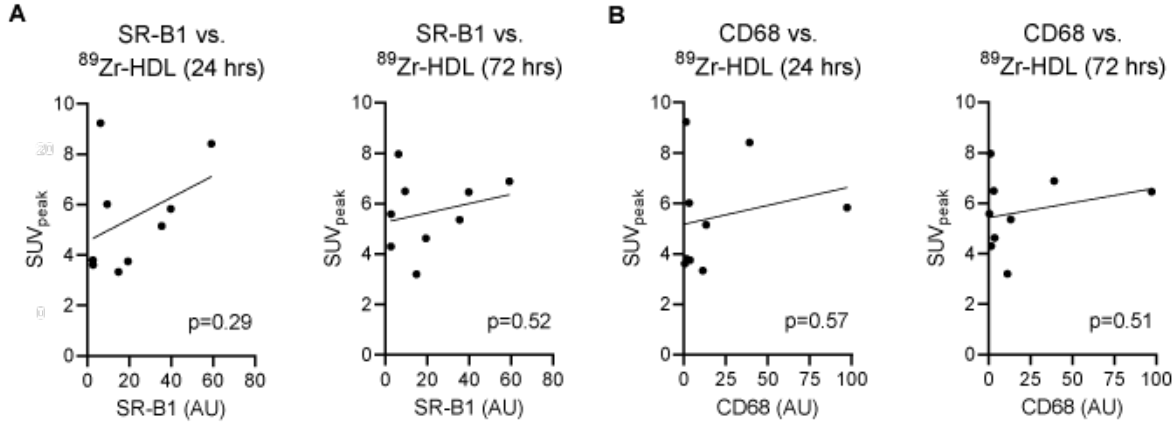

(A+B) There was no association between ^{89}Zr-HDL uptake and expression of SR-B1 and CD68.

Supplemental Table 1. Ogan-absorbed dose and residence time

Target Organ	**Mean dose**
Adrenals	0,013±0,007
Brain	0,001±0,000
Esophagus	0,048±0,013
Eyes	0,000±0,000
Gallbladder Wall	0,007±0,001
Left colon	0,024±0,002
Small Intestine	0,004±0,000
Stomach Wall	0,086±0,013
Right colon	0,025±0,002
Rectum	0,009±0,001
Heart Wall	0,008±0,001
Kidneys	0,025±0,009
Liver	0,053±0,010
Lungs	0,070±0,008
Pancreas	0,006±0,000
Prostate	0,002±0,000
Salivary Glands	0,003±0,001
Red Marrow	0,044±0,005
Osteogenic Cells	0,004±0,001
Spleen	0,011±0,004
Testes	0,011±0,002
Thymus	0,004±0,001
Thyroid	0,015±0,003
Urinary Bladder Wall	0,014±0,003
Remainder of total body	0,041±0,006
Effective Dose (mSv/MBq)	0,523±0,040
	Residence time (h)
Brain	0,403±0,088
Esophagus	0,404±0,168
Stomach	0,778±0,459
Heart	2,583±0,745
Left kidney	3,473±1,360
Liver	11,164±2,753
Left lung	1,619±0,346
Spleen	1,172±0,603
Total body	92,610±10,859